Design of Thin Circular Cylinders Under Combined Loading Conditions

E. ANTONA and G. GABRIELLI
Istituto di Progetto di Aeromobili del Politecnico di Torino, Italy

SUMMARY

The experimental results on instability of long thin circular cylinders under axial compression, bending, torsion, shear and external pressure are surveyed and the generalised structural indexes related to the latter are defined. By correlating some experimental results of other authors, the cylinder behaviour under combined load conditions and the stabilising effect of internal pressure are discussed. Formulas and diagrams were derived for the design of thin circular cylinders subjected to combined loads, such as: axial compression and pressure, bending and pressure, torsion and pressure, shear and pressure, axial compression and bending, axial compression and torsion, bending and torsion, bending and shear. In this connection, the generalised structural indexes were used to evaluate directly cylinder thickness starting from design data.

1. INTRODUCTION

Thin† circular cylinders often appear as components in aircraft and more especially in missile constructions.

The phenomena of elastic instability of thin cylindrical shells are not quite fully understood yet, even though extensive research both basic and experimental was dedicated to them by several investigators.

Among instability phenomena there are two especially — compression and

† It is specially referred here to cylinders having radius–thickness ratios higher than 300 up to 3000 approx.

bending — which show such a complicated mechanics that the results so far published are widely scattered, not to mention the striking discrepancies between many theories and experimental results.

It is well known that thin circular cylinders, as regards the length effect on instability phenomena, can be classified as short, intermediate, long and very long[1].

The very long cylinders are the ones where, under axial compression, Euler's general instability appears before local instability.

In the field of local instability, every yield stress (either normal σ or tangential τ) put in the form

$$\sigma_r = K_r \frac{\pi^2 E}{12} \left(\frac{s}{l}\right)^2 \frac{1}{1-\nu^2} \tag{1}$$

originates coefficients K_r that are a function of the length parameter Z.

The curves $K_r = K_r(Z)$ plotted a on log–log diagram appear in three zones: one with K_r constant (short cylinders), an intermediate zone of transition (intermediate cylinders) and one with K_r changing linearly (long cylinders). In the latter case we have:

$$K_r = aZ^b \tag{2}$$

where a is in general a function of s/r and b is a constant.

The values of Z separating such fields from each other depend on the stress type. However, they do not vary widely, and in particular for $Z > 100$ the cylinders always behave as long.

As such a field is the one of major practical interest, only long cylinders are considered in the present study.

It is known that in local buckling problems, after the first buckle has appeared (critical stress), the structure can generally withstand additional loads up to collapse (failure stress). In thin circular cylinders under compression and bending, however, there is a typical identity between critical and failure stresses (*i.e.* a lack of capacity to withstand loads beyond critical ones).

The majority of experimental results available for the remaining load conditions are related to failure rather than to buckling stresses[1,2].

In the present study reference is made to failure stresses.

Symbols

a	function of s/r, for any non-combined load	
b	constant, for any non-combined load	
E	Young's modulus	(kg/cm^2)
$K = \sigma \,.\, 12(1-\nu^2)(l/s)^2/\pi^2 E$		
i	structural index	(kg$^{1/2}$/cm)

I generalised structural index
l axial length of cylinder (cm)
M bending moment (kg × cm)
p pressure (kg/cm^2)

$\bar{p} = \frac{p}{E}\left(\frac{r}{s}\right)^2$ generalised pressure

P axial load (kg)
Q torque (kg × cm)
r cylinder average radius (cm)
R ratio of failure stress under combined loads and failure stress under single load
s cylinder thickness (cm)
T shear (kg)

$Z = \frac{l^2}{rs}(1-\nu^2)^{1/2}$ = length parameter

σ normal stress (kg/cm^2)
τ tangential stress (kg/cm^2)
ν Poisson's ratio

Superscripts
e external
i internal

Subscripts
c buckling
l local
M bending
0 single load
p pressure
P axial compression
Q torsion
r failure
T shear

2. Scope of the Study

For smooth thin circular cylinders, design data are generally (*see* Fig. 1):
— geometrical dimensions: length l and radius r
— applied loads: *e.g.* axial load P, bending moment M, torque Q, shear T, pressure p
— constraint conditions.

The unknowns in the design problem are:
— material
— thickness (or thickness–radius ratio)
— failure stresses.

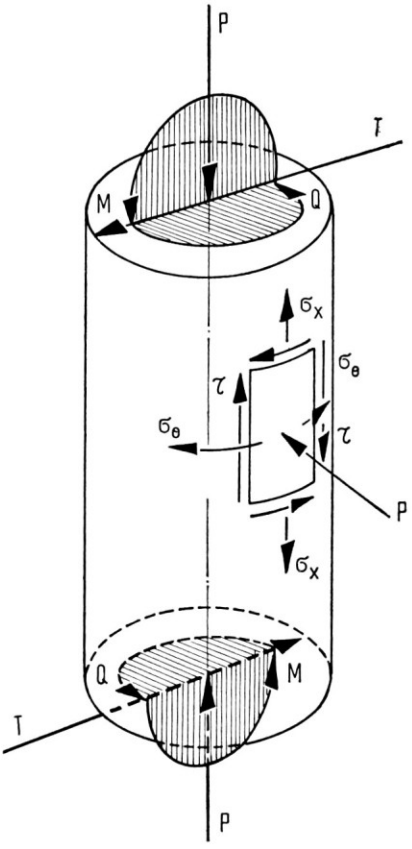

FIG. 1

The choice of the material depends on such conditions as minimum weight, transparency to radio waves, etc.

The scope of this study is to survey the experimental results so far obtained for shell instability under single and combined load conditions, and derive from them formulas and diagrams in the most generalised form. The latter can be used directly in actual design for the evaluation of cylinder thickness.

The ratio between thickness and radius being known, working stresses can easily be evaluated through direct calculation.

3. Instability of Thin Circular Cylinders

3.1. *Axial compression*

From a theoretical viewpoint, axial compression is by far the most interesting case. At one critical value of strain under axial compression, the thin circular cylinders snap into a diamond-shaped buckle, where the cylindrical surface undergoes large deformations into triangular faces.

This type of buckling shows two features:
— it appears suddenly and does not allow for loads other than the critical one
— the relevant experimental results obtained up to the present time are widely scattered.

The first attempt to see whether there was good agreement between theory and experiment was in 1930 and was not encouraging. As a matter of fact, the theoretical results so far reached in the investigation of elastic stability by small-deflection theory† gave critical stresses twice or three times larger than the experimental ones. Theory alone has not been able yet to explain fully such a phenomenon, and research is still being done. However, a few basic advances have already been made.

To take into account the macroscopic deformations, Kàrmán and Hsue-Shen[3] introduced the main second-order terms into the study of the shell elastic balance, whereas Donnell and Wan[4] introduced the effect of initial deviations from the assumed perfect geometrical shape. The theoretical problem is now being investigated by many researchers and among them we particularly mention Hoff[5,6].

Today engineers can draw only from experimental results of several investigators. As stated earlier, such results are widely scattered: Suer, Harris, Skene and Benjamin[7] by working on all known results have derived diagrams of critical stresses conservatively enveloping the 90% and 99% of experimental data. For design purposes in particular, they suggest the data at 90%. Abraham[2] reports such data in the following formula valid for $\nu = 0{\cdot}316$.

$$\sigma_{rP_0} = 0{\cdot}248 \times 10^{-7} E \frac{r}{s} + 0{\cdot}185 E \frac{s}{r} - 9{\cdot}7 \times 10^{-5} E - 1{\cdot}81 \times 10^{-12} E \left(\frac{r}{s}\right)^2 \qquad (3)$$

Poisson's ratio ν may be introduced in eqn. (3), by recalling general eqns. (1) and (2) and also considering that, for axial compression, b is equal to unity[1,7].

† Such a theory had until then proved valid for all elastic stability problems being met in engineering.

By operating in such a way, one obtains:

$$\sigma_{rP_0} = \frac{E}{\sqrt{(1-\nu^2)}}\left[0{\cdot}235 \times 10^{-7}\frac{r}{s} + 0{\cdot}1755\frac{s}{r} - 9{\cdot}2 \times 10^{-5} - 1{\cdot}72 \times 10^{-12}\left(\frac{r}{s}\right)^2\right] \tag{4}$$

This formula seems to be the most reliable in view of all experimental results and theoretical interpretations published up to the present time.

3.2. *Bending*

Instability phenomena in the portion subjected to bending loads are very similar to axial compression. Small deflection theories give values of critical stress of about 1·30 times larger than for compression. Gerard and Becker[1] attain the same result from experimental results.

Suer, Harris, Skene and Benjamin[8], similarly to what they had already done for compression, have performed a synthesis of all the experimental results, by plotting diagrams which conservatively envelop the 90% and 99% of them. Here, too, they suggest the envelope at 90%, which according to Abraham[2], may be expressed as follows:

$$\sigma_{rM_0} = \sigma_{rP_0} F\left(\frac{r}{s}\right) \tag{5}$$

The function $F = F(r/s)$ is given in Table 1.

TABLE 1

r/s	300	500	1000	1500	2000	2500	3000
$F(r/s)$	1·595	1·46	1·35	1·315	1·30	1·29	1·22

3.3. *Torsion*

Torsion instability is not so complicated, especially in theoretical investigations, as the two previous cases. The formula mostly used at present is the one reported by Abraham[2] based on the experimental results of Lundquist[9]:

$$\tau_{rQ_0} = 1{\cdot}275E\left(\frac{r}{l}\right)^{0{\cdot}46}\left(\frac{s}{r}\right)^{1{\cdot}35} \tag{6}$$

Gerard and Becker[1] have made a comparison between the theory of Batdorf, Schildcrout and Stein[10], which covers the buckling stresses, and the experimental results obtained by several authors including Lundquist. The experimental points, for the failure stress, cover a wide area (also here mean-

ing scatter); however, all of them fall below the line representing the formula. Gerard and Becker suggest the use of average values which correspond to approximately 85% of the ones given by theory. In view of what has been done by Suer, Harris, Skene and Benjamin for compression and bending[7,8], it is proposed to consider a formula for torsion, conservatively enveloping about 90% of experimental results.

Gerard and Becker[1] in plotting experimental results have used the definition of eqn. (1).

From the diagrams of Figs. 26 and 27 reported by them, one can see that the conservative envelope of the 90% of experimental points, with particular reference to the range $1000 < Z < 10{,}000$, taking $b = 0{\cdot}733$, on the basis of a graphic correlation, and a probability coefficient of 1·28, is obtained with

$$a = 0{\cdot}661$$

By recalling the definitions of Z, (eqns. (1) and (2)) the following formula is derived:

$$\tau_{rQ_0} = 0{\cdot}544 \frac{E}{(1-\nu^2)^{0{\cdot}633}} \left(\frac{r}{l}\right)^{0{\cdot}534} \left(\frac{s}{r}\right)^{1{\cdot}267} \tag{7}$$

which expresses the tangential stress of torsional failure that conservatively envelops 90% of experimental results. For radius–thickness ratios between 15 and 30 G. Gabrielli[11] has obtained failure stresses independent of l/r. The comparison of eqn. (7) with such results (Fig. 2) induces the examination of the range of l/r values, where eqn. (7) is valid. Such an examination suggests the validity of eqn. (7) is restricted to values of l/r between 0·5 and 2·5. Preti[12] has carried out torsion tests on thin circular cylinders, by bringing every structure up to buckling several times. The results related to the first applications of loads are in agreement with eqn. (7). By repeated loadings he has obtained buckling stresses gradually decreasing down to about 60% of the value obtained on the first loading (value already reached at the 4th and 5th loading). Therefore, it is to be understood that eqn. (7) applies to sound structures not previously buckled.

3.4. *Shear*

It is obviously not possible to attain a condition of pure shear (bending moment identically null) on a cylinder of finite length. Lundquist's[13] experiences, however, have shown that if the parameter M/rT is not higher than unity in any cross-section of the cylinder, failure does not appear with the typical form of bending, but with deformations mainly due to shear.

In spite of the simultaneous presence of bending, the maximum tangential failure stress (on the neutral axis), derived through the small-deflection theory, is about 1·25 times larger than failure under pure torsion.

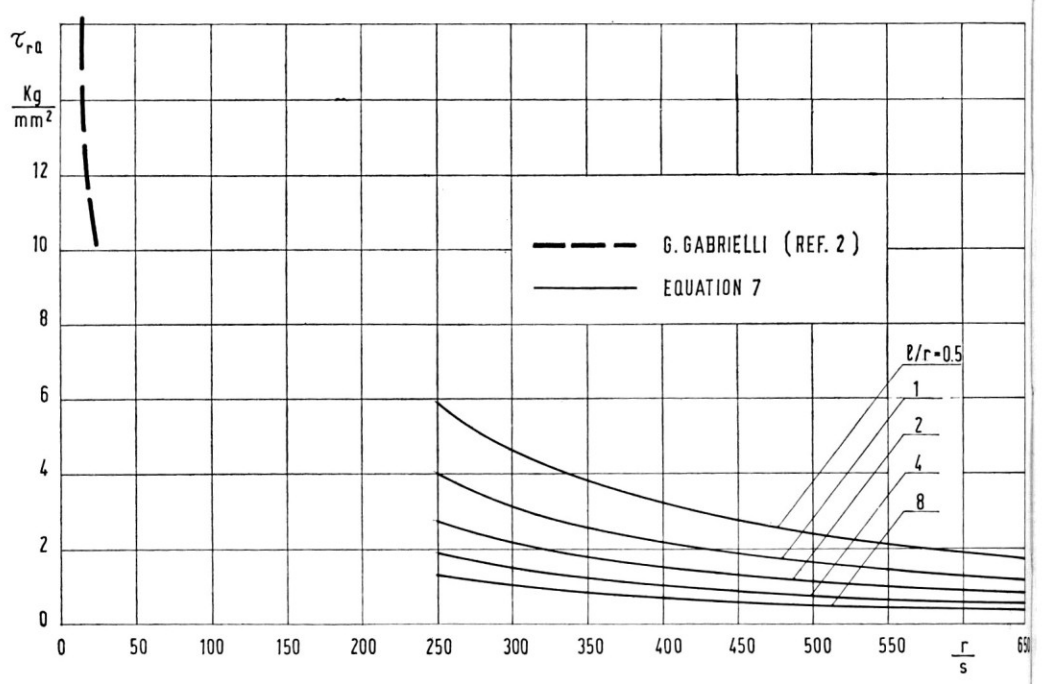

FIG. 2 — Circular cylinders under torsion

The data on pure torsion used by Lundquist for comparison are those of eqn. (6) and the 1·25 factor corresponds approximately to the average value of the shear results. As for torsion, it is proposed to consider a conservative envelope of 90% of experimental results. Furthermore it is necessary to refer the results, which according to such a conception can be derived from Lundquist's tests, not to eqn. (6) but to eqn. (7).

From a re-elaboration of Lundquist's experimental results (*see* section 5.8), the tangential failure stress conservatively enveloping 90% of experimental results can be evaluated from

$$\tau_{rT_0} = 1{\cdot}60\tau_{rQ_0} \tag{8}$$

Such a failure stress applies to the case where $M_{max}/rT \leqq 1$, which can also be considered simultaneous with other load cases.

Equation (8), even though obtained on the basis of experimental results from a single author, appears to be confirmed by the fact that pure torsion tests made by the same author show a scattering similar to the one appearing in all the available results[1]. Therefore, it seems credible that Lundquist's shear tests are also a cross-section of the scattering and conservative envelope at 90%, that could be obtained by extending experiments.

3.5. *External pressure*

Both theory and experience indicate that for long cylinders ($Z>100$) there is no difference between failure radial and hydrostatic pressures†.

Windemberg and Trilling[14] have derived, from experimental data, an equation based on the theoretical results of von Mises. For $Z>100$ failure circumferential stress is

$$\sigma_{rp_0} = 0{\cdot}855 \frac{E}{(1-\nu^2)^{0{\cdot}75}} \frac{r}{l}\left(\frac{s}{r}\right)^{1{\cdot}5} \frac{1}{1-0{\cdot}635(r/l)(s/r)^{0{\cdot}5}}$$

This relation is in excellent agreement with Batdorf's theory and Sturm's results as reported by Gerard and Becker[1], but does not appear under monomial form which is easier to handle. In order to have an expression in good agreement with the above results and valid in the field of our interest ($Z>100$ and $300<r/s<3000$) it is possible to simplify the previous equation introducing in it an average constant value for the term $0{\cdot}635(r/l)(s/r)^{0{\cdot}5}$. Operating one obtains the following expression of the failure circumferential stress:

$$\sigma_{rp_0} = 0{\cdot}88 \frac{E}{(1-\nu^2)^{0{\cdot}75}} \frac{r}{l}\left(\frac{s}{r}\right)^{1{\cdot}5} \tag{9}$$

that is valid both for radial pressure and hydrostatic pressures, which will be referred to in the subsequent considerations.

4. The Generalised Structural Indexes

In structural design the structural indexes are of great use. They have been thoroughly dealt with by G. Gabrielli[15]. For the present study it is enough to remember that the main features of the structural index are as follows:

— it covers all and only design data: loads and dimensions, *i.e.*, a typical force of the system of forces applied to a typical length of structure dimensions (shape is obviously predetermined).

— it is invariant for geometrically similar structures, of the same material and similarly loaded, and represents in a typical way the static conditions of infinite similar structures by pointing out the interrelation between applied loads and dimensions.

The major advantage of the use of the structural index in design is that it

† By radial pressure is meant a pressure applied to cylinder lateral surface only, and capable of generating in the shell the circumferential stress $\sigma_\theta = p(r/s)$ only. By hydrostatic pressure is meant a pressure applied to cylinder lateral surface and bases as well, and capable of generating other than the circumferential stress a longitudinal stress $\sigma_x = \frac{1}{2}p(r/s)$, and consequently an axial load $P = \pi r^2 p$.

allows direct calculations by using data of general validity put into the form of failure stresses as a function of the structural load itself.

In the present study a generalisation of the structural indexes relative to the cases under consideration is proposed. It is assumed that the material of the shell to be designed is known, and, by introducing the generalised structural indexes, one puts in an extremely simple and general form all the expressions of failure conditions previously presented. They allow design calculations to be made directly, even in the case of two simultaneous combined loads. To this end, interaction equations in terms of generalised structural indexes are derived, and related curves of general validity are plotted.

Equations (4), (5), (7), (8) and (9) are in the form:

$$\sigma_r = E(1-\nu^2)^m \left(\frac{l}{r}\right)^n G\left(\frac{s}{r}\right)$$

when m and n are numerical exponents and $G(s/r)$ is a function depending on the case being considered.

Recalling the definitions of structural indexes[15] also reported in Table 2, such an equation can be put in the form

$$i_r^2 = E(1-\nu^2)^m \left(\frac{l}{r}\right)^n G^*\left(\frac{s}{r}\right)$$

where

$$G^*\left(\frac{s}{r}\right) = \frac{s}{r} G\left(\frac{s}{r}\right)$$

Let us consider the index I_r, such that

$$I_r^2 = i_r^2 E^{-1}(1-\nu^2)^{-m} \left(\frac{l}{r}\right)^{-n}$$

The preceding equation becomes

$$I_r^2 = G^*\left(\frac{s}{r}\right)$$

In such an equation on the left-hand side the index contains all and only design data (loads, external dimensions, shape) and the values to be chosen at design (Young's modulus, Poisson's ratio). On the right-hand side there is a function of the single unknown of the problem, s/r.

The equation itself, in its formal validity, is invariant for any instablity problem of long thin cylinders under noncombined load conditions.

The various expressions of $G^*(s/r)$ related to individual cases are also invariants for the same cylinders under the relevant load conditions.

Table 2 gives the definitions of both structural indexes and generalised structural indexes for the load cases considered.

TABLE 2

Load	*Structural index* $kg^{1/2}/cm$	*Generalised structural index*
Axial compression	$i_p = \sqrt{\frac{P}{2\pi r^2}} = \sqrt{\sigma}\ \sqrt{(s/r)}$	$I_P = \sqrt{\frac{P}{2\pi r^2}} \cdot \sqrt{\frac{(1-\nu^2)^{0\cdot5}}{E}}$
Bending	$I_M = \sqrt{\frac{M}{\pi r^3}} = \sqrt{\sigma_{\max}}\ \sqrt{(s/r)}$	$I_M = \sqrt{\frac{M}{\pi r^3}} \cdot \sqrt{\frac{(1-\nu^2)^{0\cdot5}}{E}}$
Torsion	$i_Q = \sqrt{\frac{Q}{2\pi r^3}} = \sqrt{\tau}\ \sqrt{(s/r)}$	$I_Q = \sqrt{\frac{Q}{2\pi r^3}} \cdot \sqrt{\frac{(1-\nu^2)^{0\cdot663}}{E}} \left(\frac{1}{r}\right)^{0\cdot267}$
Shear	$i_T = \sqrt{\frac{T}{\pi r^2}} = \sqrt{\tau_{\max}}\ \sqrt{(s/r)}$	$I_T = \sqrt{\frac{T}{\pi r^2}} \cdot \sqrt{\frac{(1-\nu^2)^{0\cdot663}}{E}} \left(\frac{1}{r}\right)^{0\cdot267}$
External pressure	$i_p = \sqrt{p} = \sqrt{\sigma}\ \sqrt{(s/r)}$	$I_p^e = \sqrt{p} \sqrt{\frac{(1-\nu^2)^{0\cdot75}}{E}} \left(\frac{1}{r}\right)^{0\cdot5}$
Internal pressure		$I_p^i = \sqrt{p}\ \sqrt{(1/E)}$

Table 3 gives the expressions for the generalised failure structural indexes derived from eqns. (4), (5), (7), (8) and (9).

TABLE 3

Load	*Failure generalised structural index*
Axial compression	$I^2_{rP_0} = 0\cdot235 \times 10^{-7} + 0\cdot1755\left(\frac{s}{r}\right)^2 - 9\cdot2 \times 10^{-5}\frac{s}{r} - 1\cdot72 \times 10^{-12}\left(\frac{s}{r}\right)^{-1}$
Bending	$I^2_{rM_0} = F\left(\frac{s}{r}\right) I^2_{rP_0}$
Torsion	$I^2_{rQ_0} = 0\cdot544\left(\frac{s}{r}\right)^{2\cdot267}$
Shear	$I^2_{rT_0} = 0\cdot870\left(\frac{s}{r}\right)^{2\cdot267}$
Radial or hydrostatic external pressure	$I^{e2}_{rP_0} = 0\cdot88\left(\frac{s}{r}\right)^{2\cdot5}$

Figure 3 gives the generalised structural index in the field of interest at failure stresses under noncombined load conditions plotted against r/s.

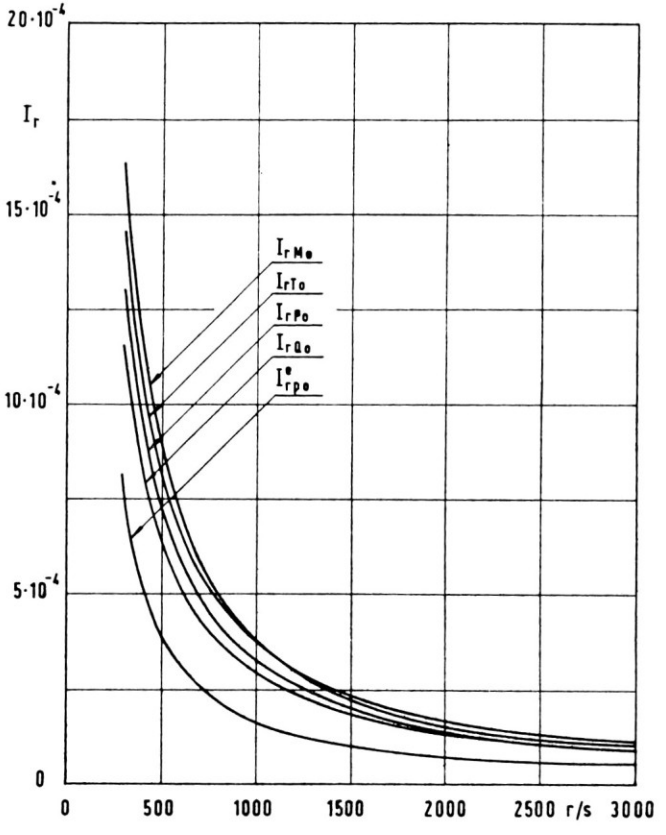

FIG. 3 — Failure values of generalised indexes for noncombined loading conditions

5. THE INTERACTION BETWEEN COMBINED LOADS

5.1. *Axial compression and pressure*

Internal pressure has a stabilising effect on the compression instability phenomena. The nature of such an effect is very involved and not fully understood.

Suer, Harris, Skene and Benjamin[7] have worked out the available experimental results by calculating curves conservatively enveloping the 90% . Abraham[2], for $\nu = 0{\cdot}316$, reports such results in the form:

$$\frac{\Delta\sigma_{rP}}{E}\frac{r}{s} = \frac{\bar{p}}{0{\cdot}7+4{\cdot}2\bar{p}}$$

where

$$\bar{p} = \frac{p}{E}\left(\frac{r}{s}\right)^2$$

As for single compression, one can introduce Poisson's ratio. Following section 3.1, one obtains

$$\Delta\sigma_{rP}\frac{\sqrt{(1-\nu^2)}}{E}\frac{r}{s} = \frac{\bar{p}}{0{\cdot}737+4{\cdot}425\bar{p}} \tag{10}$$

It should be noted that according to eqn. (10), the maximum stresses assume values equal to 2/3 of the ones given by the small-deflection theory, of which about 1/3 is made up by σ_{rP_0} and 1/3 by $\Delta\sigma_{rP}$†. The impossibility of reaching, through internal pressure stability, the value given by the small-deflection theory is an anomaly in the instability phenomena of this type. For example, in cylinder bending, in cone compression and bending such a value is normally reached.

Weingarten, Morgan and Seide[16], have obtained on polyesther resin cylinders with internal pressure, failure stresses which asymptotically approach the ones in small-deflection theory. They also observed that under the combined effect of internal pressure and axial load, as soon as the elastic limit is reached a drop by $\Delta\sigma_{rP}$ will be recorded. In the case of the polyesther resin, this happens for high values of $\bar{p}$, when σ_{rP} has already virtually reached the theoretical value.

For materials used in the tests by Suer, Harris, Skene and Benjamin (steels, aluminium alloys, etc.), this happens before such a value is reached. However, eqn. (10) gives a good interpretation of the initial stretches of the $\Delta\sigma_{rP}$ curves in terms of $\bar{p}$ obtained by Weingarten, Morgan and Seide. It is used here, by assuming that it is conservative for materials with high elastic limit at the higher values of $\bar{p}$.

Gerard and Becker[1] and Abraham[2] report the following equation for the interaction between axial compression and external pressure:

$$R_P + R_p = 1 \tag{11}$$

5.2. *Bending and pressure*

Internal pressure also has a stabilising effect in bending. Suer, Harris, Skene and Benjamin[8], by operating on test data where only radial pressure was present, have determined the curve conservatively enveloping 90% of experimental results. It is deemed proper to suggest a representation of such a curve by the following equation:

† According to the small-deflection theory, one has $\sigma_{rP_0} \cong 0{\cdot}6E(s/r)$, $\Delta\sigma_{rP_0} = 0$.

$$\Delta\sigma_{rM}\frac{\sqrt{(1-\nu^2)}\,r}{E\quad s}=0{\cdot}362\bar{p}^{0{\cdot}223} \tag{12}$$

valid for radial pressure and for values of $\bar{p}$ up to about 8.

Gerard and Becker[1] and Abraham[2] for the interaction between bending and external pressure report an equation similar to eqn. (11).

$$R_M+R_p=1 \tag{13}$$

5.3. *Torsion and pressure*

According to Crate, Batdorf and Baab[17] and Abraham[2], the following interaction law between torsion and pressure is valid both for external and internal pressures:

$$R_Q^2+R_p=1 \tag{14}$$

where R_p is related to the critical external pressure and where for external and internal pressures, respectively

$$R_p=R_p^e;\quad R_p=-R_p^i$$

For external pressure, eqn. (14) applies both for hydrostatic and radial pressures, while it is thought that for internal pressure it applies for hydrostatic pressure only.

5.4. *Shear and pressure*

Abraham[2] reports a law similar to eqn. (2):

$$R_T^2+R_p=1 \tag{15}$$

where R_p is related to the critical external pressure and where for external and internal pressures, respectively

$$R_p=R_p^e;\quad R_p=-R_p^i$$

It is thought that eqn. (15) applies for both hydrostatic and radial pressures in the case of external pressure, and only for hydrostatic pressure in the case of internal pressure.

5.5. *Axial compression and bending*

According to Bruhn[18], Gerard and Becker[1] and Abraham [2], the following interaction law is valid

$$R_P+R_M=1 \tag{16}$$

5.6. *Axial compression and torsion*

Abraham[2] reports the following interaction law

$$R_P + R_Q^2 = 1 \tag{17}$$

5.7. *Bending and torsion*

Gerard and Becker report the following interaction law

$$R_M^{1.5} + R_Q^2 = 1 \tag{18}$$

For ratios r/s between 15 and 30 G. Gabrielli[11] has found an interaction law similar to eqn. (18).

5.8. *Bending and shear*

Simultaneous bending and shear has been investigated experimentally by Lundquist. He also derived a diagram taking into account the interaction between both loads and suggested its use in design. Such a diagram was derived with the following linear interaction between the local compressive stresses due to bending and shear stresses, both being calculated on the basis of St. Venant's hypothesis:

$$R_{M_1} + R_{T_1} = 1$$

and by taking as failure stresses under separate load conditions the ones obtained by Lundquist himself[9,19].

Lundquist compared *a posteriori* the results of this theory with the experimental results, and found them to be in fair agreement.

Since Lundquist[13] has largely reported the results of experimental measurements, it does not seem useless here to do a complete re-elaboration of them, where the conservative envelope criterion of about 90% of results is introduced.

To this end, for bending moment and compression stresses, the section with maximum moment is assumed as reference.

In such a section, the generalised failure structural indexes (*see* section 4) I_{rM} and I_{rT} are evaluated.

Once the generalised structural indexes relating to the noncombined load conditions I_{rM_0} and I_{rQ_0} have been evaluated, one plots, on an x- and y-plane diagram, the points:

$$\left(\frac{I_{rM}}{I_{rM_0}}\right)^2, \quad \left(\frac{I_{rT}}{I_{rQ_0}}\right)^2$$

Such points, due to the very nature of the generalised structural indexes, make abstraction both from the geometrical ratios l/r, r/s and the material

characteristics ν and E. They are, instead, affected by scattering, which, as stated earlier, interests the results related both to bending and shear, and express the interaction between both types of loads. Under this form, Lundquist's results may be interpreted with the aid of the envelope criterion. It is to be noted that if, from test results, one wants to draw general conclusions from cylinders of different materials (presently, however, the literature known to us only reports Lundquist's results), the form here suggested is the most suitable.

The points obtained in the above way are reported in Fig. 4.

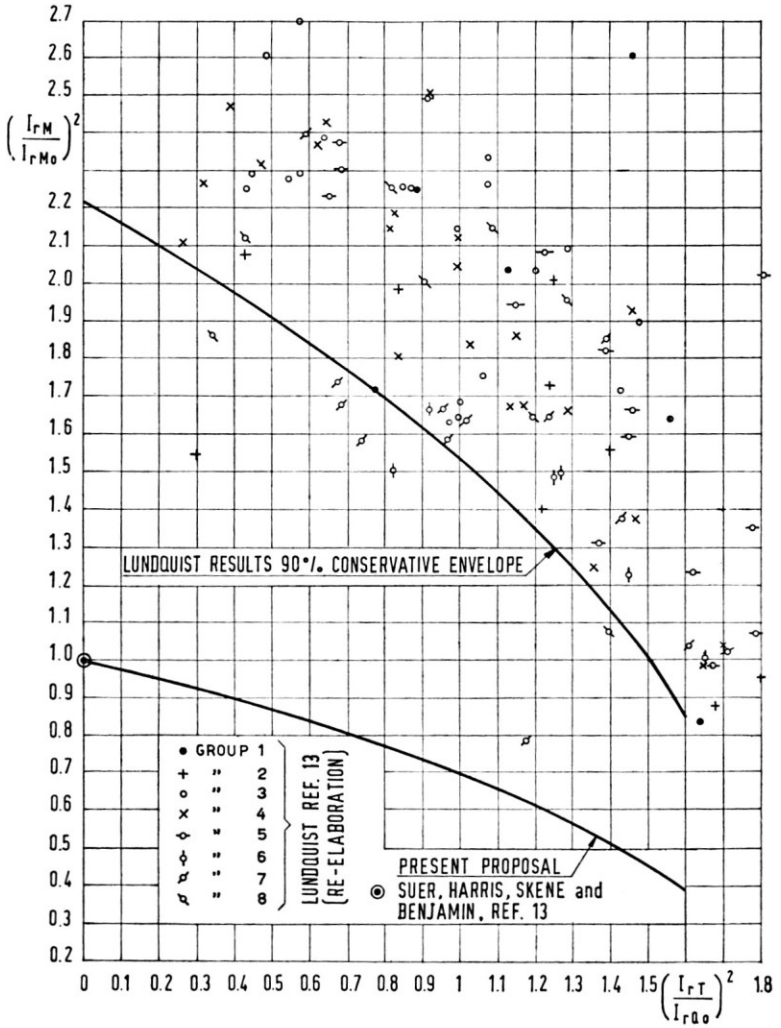

FIG. 4

From this, one can see that a conservative envelope of experimental results virtually ends at $(I_{rT}/I_{r_{Q0}})^2 = 1{\cdot}6$.

When I_{rT} tends toward zero, the envelope itself gives values of I_{rM}/I_{rM_0} higher than unity. This means that Lundquist's experience on bending failure, have a conservative envelope higher than that of Suer, Harris, Skene, and Benjamin who operated on a larger range of experimental results. In order to take into account the results of these authors, it is proposed to modify the interaction curve obtained from the re-elaboration of Lundquist's data, as shown in Fig. 4.

The proposed interaction curve is represented with good approximation by the following equation:

$$\left\{\frac{1}{0{\cdot}61}\left[\left(\frac{I_{rM}}{I_{rM_0}}\right)^2 - 0{\cdot}39\right]\right\}^{1{\cdot}2} + \left[\frac{I_{rT}}{I_{rQ_0}\sqrt{1{\cdot}6}}\right]^{2{\cdot}4} = 1 \tag{19}$$

It was obtained by reducing all ordinates I_{rM}/I_{rM_0} according to the ratio $(I_{rM}/I_{rM_0})_{IrT=0}$.

6. Design Formulas and Diagrams for Two Combined Loads

In this section, the interaction eqns. (10) to (19) introducing the generalised structural indexes defined under section 4 are put in the following form:

$$f\left(\frac{I_{rA}}{I_{rA_0}}, \frac{I_{rB}}{I_{rB_0}}\right) = 0 \tag{20}$$

where A and B indicate two general cases of load.

The structural indexes I_{rA_0} and I_{rB_0} are, as we have seen, functions of r/s (section 4). Such functions, for the cases being examined, are given in Table 3.

Therefore, eqn. (20), may be thought of as a function

$$f'(I_{rA}, I_{rB}, r/s) = 0 \tag{20'}$$

and the curves $I_{rA} = I_{rA}(I_{rB})$ for $r/s = \text{const}$ may be plotted on x- and y-axes.

Equations (20) and (20′) are invariant for long thin cylinders of isotropic material. With the related diagrams, one can immediately, and through direct calculation, design any circular long thin cylinder of isotropic material subjected to combined loads. It is sufficient to enter the diagram relating to the desired load combination with the values I_{rA} and I_{rB} and determine the value of r/s.

The formulas of section 3 also determine failure stresses through direct evaluation.

The diagrams also give immediate verification. In fact, if s/r is known, it will be enough to intersect the corresponding curve with the straight line

from the origin passing through the point (I_A, I_B) which is evaluated from the ultimate loads. Such a point gives the generalised failure structural indexes (I_{rA}, I_{rB}). The reserve factor may be evaluated as follows:

$$F.R. = \frac{I_{rA}^2}{I_A^2} = \frac{I_{rB}^2}{I_B^2}$$

6.1. *Axial compression and pressure*

Failure stress under pure compression is given by eqn. (4).

Recalling eqn. (10), the failure stress under compression in the case of simultaneous internal pressure is:

$$\sigma_{rP^*} = \sigma_{rP_0} + \frac{E}{\sqrt{(1-\nu^2)}} \frac{s}{r} \frac{\bar{p}}{0{\cdot}737 + 4{\cdot}425\bar{p}} \tag{21}$$

where P^* must be considered for hydrostatic pressure and

$$\bar{p} = \frac{p}{E}\left(\frac{r}{s}\right)^2 \qquad \text{and} \qquad P^* = P - p\pi r^2$$

Passing to the generalised structural indexes, one has

$$I_{rP^*}^2 = \sigma_{rP^*} \frac{\sqrt{(1-\nu^2)}}{E} \frac{s}{r}$$

and ultimately

$$I_{rP^*}^2 = I_{rP_0}^2 + \frac{I_{rp}^{i2}}{0{\cdot}737 + 4{\cdot}425 I_{rp}^{i2}(r/s)^2} \tag{22}$$

Equation (22) is plotted in Fig. 5(*a*).

For external pressure, the interaction equation under the form of generalised structural indexes has the simple expression

$$\frac{I_{rP}^2}{I_{rP_0}^2} + \frac{I_{rp}^{e2}}{I_{rp_0}^{e2}} = 1 \tag{23}$$

as it is easily demonstrated by recalling eqn. (11).

Equation (23) is plotted in Fig. 5(*b*).

6.2. *Bending and pressure*

For internal and radial pressure, by operating similarly to compression, one obtains:

$$\sigma_{rM} = \sigma_{rM_0} + \frac{E}{\sqrt{(1-\nu^2)}} \frac{s}{r} 0{\cdot}362 \left[\frac{p}{E}\left(\frac{r}{s}\right)^2\right]^{0{\cdot}223}$$

from which

$$I_{rM}^2 = I_{rM_0}^2 + 0{\cdot}362\left(\frac{s}{r}\right)^2 \left[I_{rp}^{i2}\left(\frac{r}{s}\right)^2\right]^{0{\cdot}223} \tag{24}$$

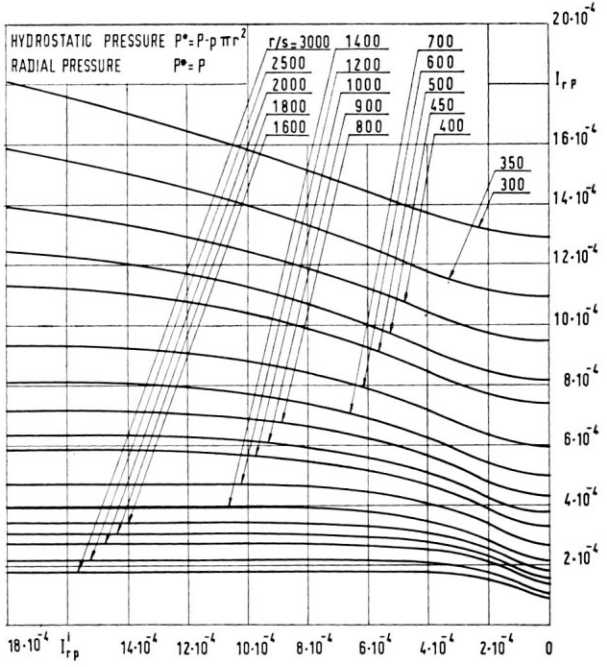

$$I_{rP^*} = \sqrt{\frac{P^*}{2\pi r^2}} \sqrt{\frac{(1-\nu^2)^{0.5}}{E}} \qquad I^i_{rp} = \sqrt{p} \sqrt{\frac{1}{E}}$$

FIG. 5(*a*) — Axial compression and internal pressure

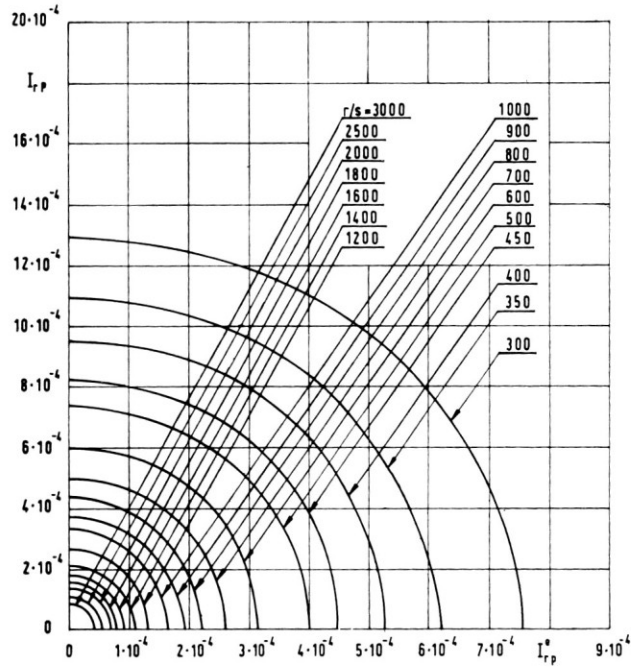

$$I_{rP} = \sqrt{\frac{P}{2\pi r^2}} \sqrt{\frac{(1-\nu^2)^{0.5}}{E}} \qquad I^e_{rp} = \sqrt{p} \sqrt{\frac{(1-\nu^2)^{0.75}}{E}} \left(\frac{l}{r}\right)^{0.5}$$

FIG. 5(*b*) — Axial compression and external pressure

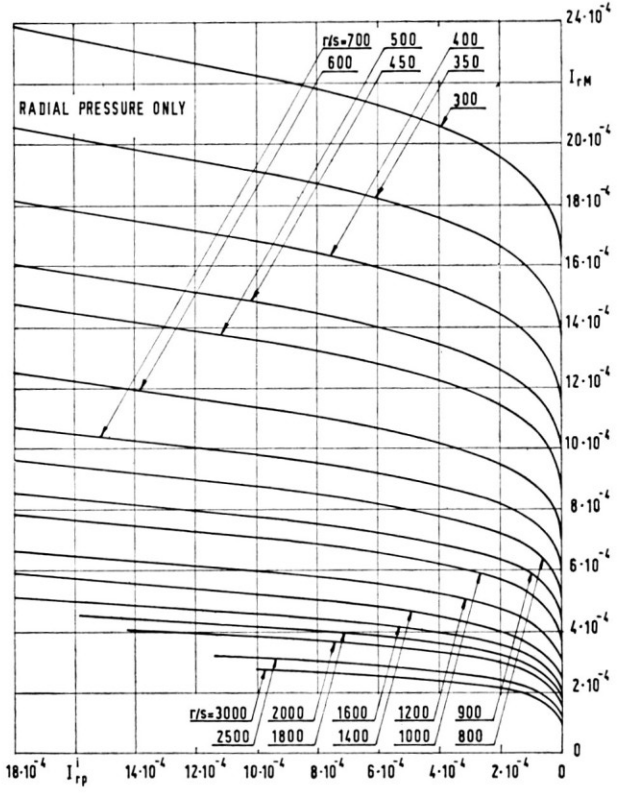

$$I_{rM} = \sqrt{\frac{M}{\pi r^3}} \sqrt{\frac{(1-\nu^2)^{0.5}}{E}} \qquad I^i_{rp} = \sqrt{p} \sqrt{\frac{1}{E}}$$

FIG. 6(*a*) — Bending and internal pressure

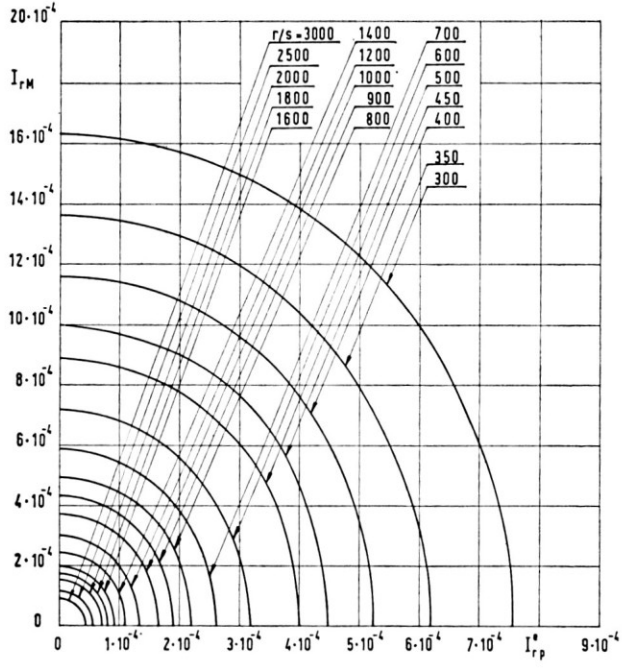

$$I_{rM} = \sqrt{\frac{M}{\pi r^3}} \sqrt{\frac{(1-\nu^2)^{0.5}}{E}} \qquad I^e_{rp} = \sqrt{p} \sqrt{\frac{(1-\nu^2)^{0.75}}{E}} \left(\frac{l}{r}\right)^{0.5}$$

FIG. 6(*b*) — Bending and external pressure

Equation (24) is plotted in Fig. 6(*a*). The curves are broken where the value of $\bar{p}=8$ is reached.

For external pressure one has, as is easily shown:

$$\frac{I_{rM}^2}{I_{rM_0}^2}+\frac{I_{rp}^{e2}}{I_{rp_0}^{e2}}=1 \tag{25}$$

Equation (25) is plotted in Fig. 6(*b*).

6.3. *Torsion and pressure*

For external and internal pressures, respectively, one has, as is easily shown

$$\frac{I_{rQ}^4}{I_{rQ_0}^4}+\frac{I_{rp}^2}{I_{rp_0}^{e2}}=1 \tag{26}$$

$$I_{rp}^2=I_{rp}^{e2}\,;\quad I_{rp}^2=-I_{rp}^{i2}$$

Equation (26) is plotted in Figs. 7(*a*) and 7(*b*).

6.4. *Shear and pressure*

For external and internal pressures, respectively, one has, as is easily shown

$$\frac{I_{rT}^4}{I_{rT_0}^4}+\frac{I_{rp}^2}{I_{rp_0}^{e2}}=1 \tag{27}$$

$$I_{rp}^2=I_{rp}^{e2}\,;\quad I_{rp}^2=-I_{rp}^{i2}$$

Equation (27) is plotted in Figs. 8(*a*) and 8(*b*).

6.5. *Axial compression and bending*

One has, as is easily shown

$$\frac{I_{rP}^2}{I_{rP_0}^2}+\frac{I_{rM}^2}{I_{rM_0}^2}=1 \tag{28}$$

Equation (28) is plotted in Fig. 9.

6.6. *Axial compression and torsion*

One has, as is easily shown

$$\frac{I_{rP}^2}{I_{rP_0}^2}+\frac{I_{rQ}^4}{I_{rQ_0}^4}=1 \tag{29}$$

Equation (29) is plotted in Fig. 10.

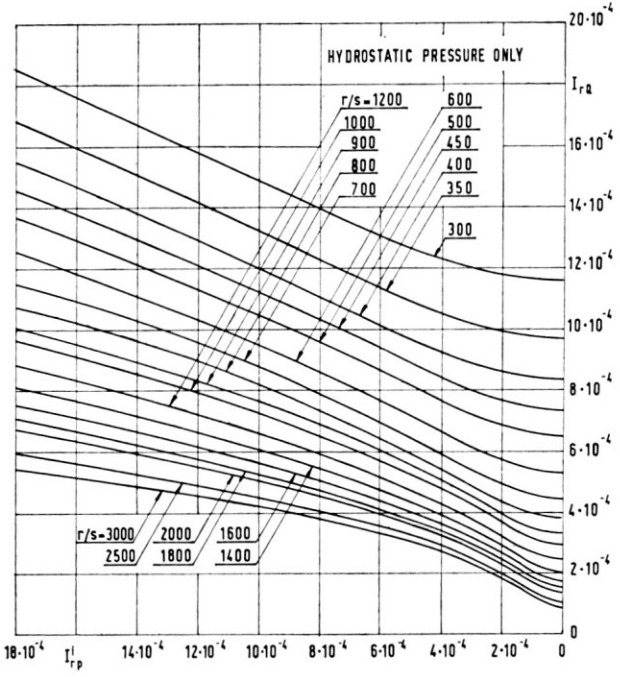

$$I_{rQ} = \sqrt{\frac{Q}{2\pi r^3}} \sqrt{\frac{(1-\nu^2)^{0.663}}{E}} \left(\frac{l}{r}\right)^{0.267} \qquad I^i_{rp} = \sqrt{p} \sqrt{\frac{1}{E}}$$

FIG. 7(*a*) — Torsion and internal pressure

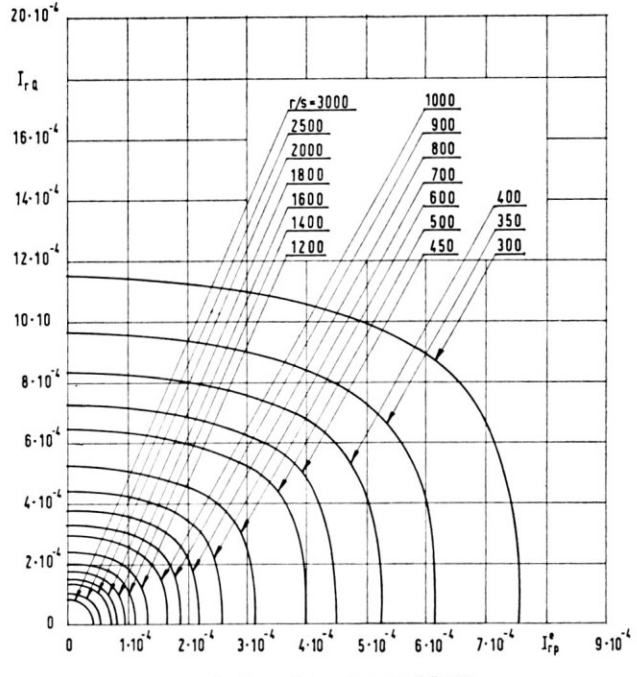

$$I_{rQ} = \sqrt{\frac{Q}{2\pi r^3}} \sqrt{\frac{(1-\nu^2)^{0.663}}{E}} \left(\frac{l}{r}\right)^{0.2}$$

$$I^e_{rp} = \sqrt{p} \sqrt{\frac{(1-\nu^2)^{0.7}}{E}} \left(\frac{l}{r}\right)^{0.5}$$

FIG. 7(*b*) — Torsion and external pressure

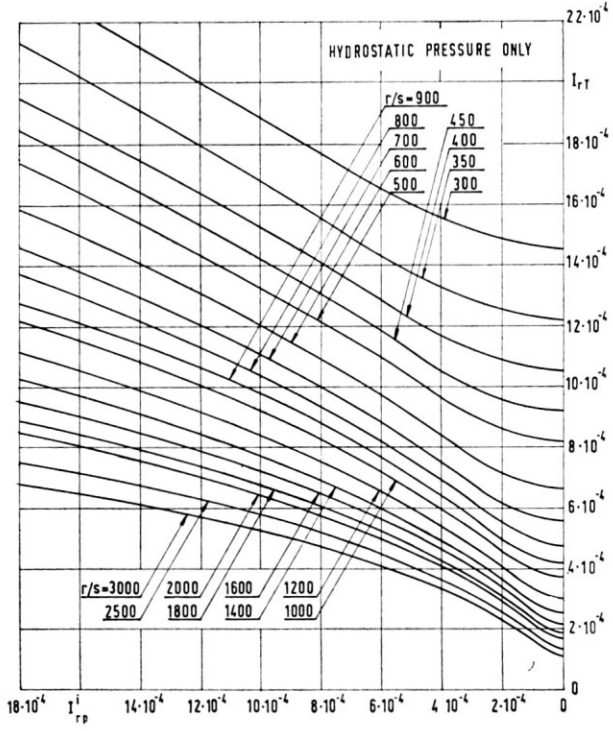

$$I_{rT}=\sqrt{\frac{T}{\pi r^2}}\sqrt{\frac{(1-\nu^2)^{0.663}}{E}}\left(\frac{l}{r}\right)^{0.267} \qquad I^i_{rp}=\sqrt{p}\sqrt{\frac{1}{E}}$$

FIG. 8(*a*) — Shear and internal pressure

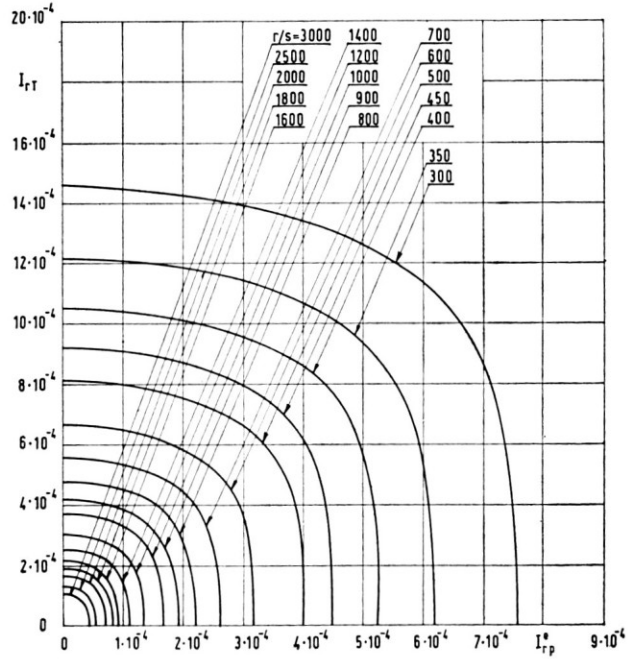

$$I_{rT}=\sqrt{\frac{T}{\pi r^2}}\sqrt{\frac{(1-\nu^2)^{0.663}}{E}}\left(\frac{l}{r}\right)^{0.267}$$

$$I^e_{rp}=\sqrt{p}\sqrt{\frac{(1-\nu^2)^{0.75}}{E}}\left(\frac{l}{r}\right)^{0.5}$$

FIG. 8(*b*) — Shear and external pressure

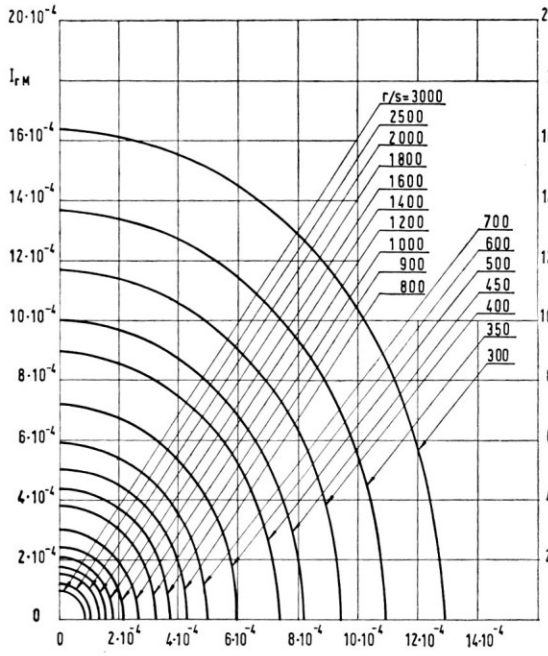

$$I_{rM} = \sqrt{\frac{M}{\pi r^3}} \sqrt{\frac{(1-\nu^2)^{0.5}}{E}}$$

$$I_{rP} = \sqrt{\frac{P}{2\pi r^2}} \sqrt{\frac{(1-\nu^2)^{0.5}}{E}}$$

FIG. 9 — Axial compression and bending

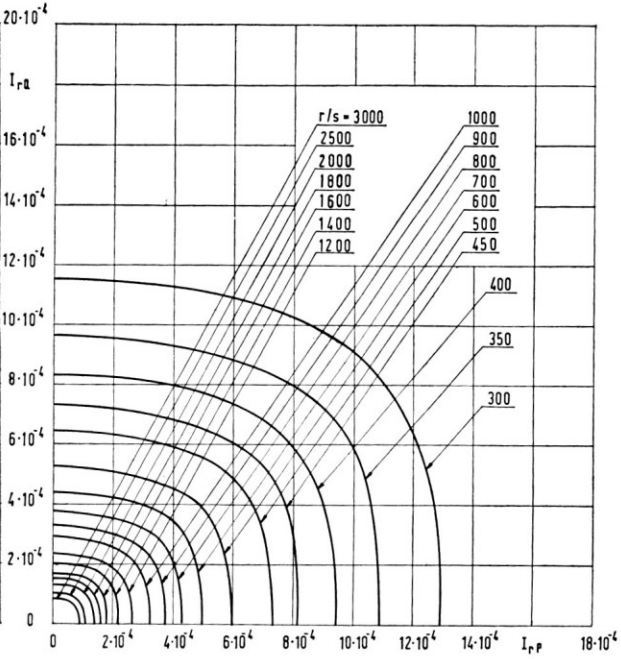

$$I_{rQ} = \sqrt{\frac{Q}{2\pi r^3}} \sqrt{\frac{(1-\nu^2)^{0.663}}{E}} \left(\frac{l}{r}\right)^{0.267}$$

$$I_{rP} = \sqrt{\frac{P}{2\pi r^2}} \sqrt{\frac{(1-\nu^2)^{0.5}}{E}}$$

FIG. 10 — Torsion and axial compression

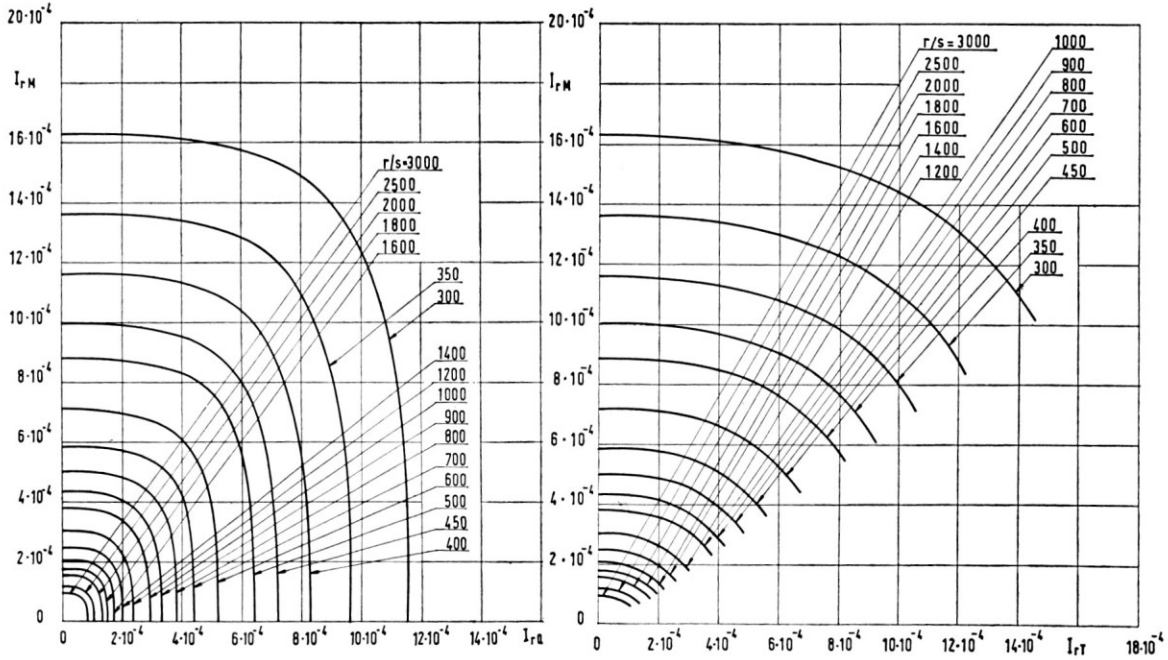

$$I_{rM} = \sqrt{\frac{M}{\pi r^3}} \sqrt{\frac{(1-\nu^2)^{0.5}}{E}}$$

$$I_{rQ} = \sqrt{\frac{Q}{2\pi r^3}} \sqrt{\frac{(1-\nu^2)^{0.663}}{E}} \left(\frac{l}{r}\right)^{0.267}$$

FIG. 11 — Bending and Torsion

$$I_{rM} = \sqrt{\frac{M}{\pi r^3}} \sqrt{\frac{(1-\nu^2)^{0.5}}{E}}$$

$$I_{rT} = \sqrt{\frac{T}{\pi r^3}} \sqrt{\frac{(1-\nu^2)^{0.663}}{E}} \left(\frac{l}{r}\right)^{0.267}$$

FIG. 12 — Bending and shear

6.7. *Bending and torsion*

One has, as is easily shown

$$\frac{I_{rM}^3}{I_{rM_0}^3} + \frac{I_{rQ}^4}{I_{rQ_0}^4} = 1 \tag{30}$$

Equation (30) is plotted in Fig. 11.

6.8. *Bending and shear*

As shown in section 5.8, eqn. (19) is valid

$$\left\{\frac{1}{0{\cdot}61}\left[\left(\frac{I_{rM}}{I_{rM_0}}\right)^2 - 0{\cdot}39\right]\right\}^{1{\cdot}2} + \left(\frac{I_{rT}}{I_{rQ_0}\sqrt{1{\cdot}6}}\right)^{2{\cdot}4} = 1$$

In this equation, I_{rM} is assumed to be calculated for the section of maximum moment.

Equation (19) is plotted in Fig. 12.

References

(1) Gerard, G., Becker, H., 'Buckling of Curved Plates and Shells,' NACA, Tech. Note 3783, 1957.

(2) Abraham, L. H., *Structural Design of Missiles and Spacecraft*, McGraw-Hill Book Company Inc., 1962.

(3) von Kármán, Theodore, Hsue-Shen, 'The Buckling of Thin Cylindrical Shells under Axial Compression,' *J. Aero. Sci.*, June 1941.

(4) Donnell, L. H., Wan, C. C., 'Effect of Imperfections on Buckling of Thin Cylinders and Columns under Axial Compression,' *J. Appl. Mechanics*, March 1950.

(5) Hoff, Nicholas J., 'Buckling of Thin Shells,' Aerospace Symposium Honoring von Kàrmán 80th, May 1961.

(6) Hoff, Nicholas J., 'Quelques nouveaux résultats de recherches sur le flambage des coques cylindriques,' VII Congrès Aéronautique International, Paris, Juin 1965.

(7) Suer, H. S., Harris, L. H., Skene, W. T., Benjamin, R. J., 'The Stability of Thin-walled Unstiffened Circular Cylinders under Axial Compression Including the Effects of Internal Pressure,' *J. Aero. Sci.*, August 1957.

(8) Suer, H. S., Harris, L. H., Skene, W. T., Benjamin, R. J., 'The Bending Stability of Thin-walled Unstiffened Circular Cylinders Including the Effects of Internal Pressure,' *J. Aero. Sci.*, May 1958.

(9) Lundquist, Eugene E., 'Strength Tests on Thin-walled Duralumin Cylinders in Torsion,' NACA Tech. Note 427, 1932.

(10) Batdorf, S. B., Stein, Manuel, Schildcrout, Murry, 'Critical Stress of Thin-walled Cylinders in Torsion,' NACA Tech. Note 1344, 1947.

(11) Gabrielli, Giuseppe, 'Sul comportamento dei tubi sottili in dural assoggettati a flessione, torsione e sulle loro applicazioni nella costruzione degli aeromobili, *l'Aerotecnica* XII, fasc. 12, 1932.

(12) PRETI, ERMENEGILDO, 'Prove di torsione su cilindri circolari a parete sottile,' Rendiconti dell'Istituto Lombardo di Scienze e Lettere A 99, 1965.
(13) LUNDQUIST, EUGENE E., 'Strength Tests of Thin-walled Duralumin Cylinders in Combined Transverse Shear and Bending,' NACA Tech. Note 523, 1935.
(14) WINDENBERG, D. F., TRILLING, C., 'Collapse by Instability of Thin Cylindrical Shells under External Pressure,' Trans. of ASME, November 1934.
(15) GABRIELLI, GIUSEPPE, 'Lezioni sulla Scienza del Progetto degli Aeromobili,' Ed. Levrotto e Bella, Torino 1961.
(16) WEINGARTEN, V. I., MORGAN, E. J., SEIDE, P., 'Elastic Stability of thin-walled cylindrical and conical shells under combined internal pressure and axial compression,' *AIAA Journal*, June 1965.
(17) CRATE, HAROLD, BATDORF, S. B., BAAB, G. W., 'The Effect of Internal Pressure on the Buckling Stress of Thin-walled Circular Cylinders under Torsion,' NACA Wartime Rept. L–67, May 1944.
(18) BRUHN, E. F., 'Tests on Thin-walled Celluloid Cylinders to Determine the Interaction Curves under Combined Bending Torsion and Compression or Tension Loads,' NACA Tech. Note 1951, 1945.
(19) LUNDQUIST, EUGENE E., 'Strength Tests on Thin-walled Duralumin Cylinders in Pure Bending,' NACA Tech. Note 479, 1933.

DISCUSSION

Prof. Josef Singer (Dept. of Aeronautical Engineering, Technion Israel Institute of Technology, Haifa, Israel): I feel that data on which empirical interaction curves for buckling under combined loading are based is not very satisfactory. Most empirical interaction curves are based on tests in which each specimen is subjected to a particular combination of loads, and the critical loads are compared to single load reference points obtained on other specimens. The resulting large scatter is mostly due to the differences between the specimens. Less scatter can be obtained by repeated buckling of the same specimen over the complete interaction range, if sufficient care is taken. For example, in a recent series of tests on buckling of conical shells under combined loading of axial compression, torsion and external pressure†, one specimen was buckled 162 times with a rate of decrease in buckling torque of 0·05% per test and 0·2% in buckling pressure per test.

Hence a plea is made for new and better tests to re-evaluate existing empirical interaction formulae.

E. Antona and G. Gabrielli: It is certainly desirable that the experimental research on the combined loads interaction will be improved and extended to obtain a very large amount of new data concerning all the loading conditions.

It is our opinion that the basic point for the experimental work is to have

† SINGER, J., BERKOVITZ, A., WELLER, T., ISHAI, O., BARUCH, M., HARARI, O., 'Experimental and Theoretical Studies on Buckling of Conical and Cylindrical Shells under combined Loading,' TAE Report 48, Technion Research and Development Foundation, Haifa, Israel, June 1966.

a large number of experimental data for a statistical analysis. We are however doubtful of the value of using only one specimen for repeated buckling tests under combined loads. We think that this procedure would not be useful in reducing the scattering of experimental results arising from different behaviour of many specimens. On this subject we will consult the reference cited by the discussor.

D. J. Johns (Reader in Aeronautical Engineering, University of Technology, Loughborough, Leics., U.K.): The authors, in section 3.2, have quoted the theoretical result for isotropic shells that the critical bending stress is about 1·3 times that for uniform compression. It has been shown more recently† that if sufficient modes are included in the bending analysis then these critical stresses are generally equal.

The speaker has performed calculations for shells subjected to uniform bending moment or linear bending moment (i.e. due to transverse end load) and by choosing a few modal forms which emphasise the (anticipated) local nature of the buckling it has been possible to deduce the following general implication, namely linear buckling of a circular cylindrical shell due to a non-uniform axial compressive stress distribution will occur at a load level where the maximum local stress equals the uniform stress for buckling.

It is known that the corresponding experimental buckling stress levels are usually significantly lower than the values based on linear small deflection theory, and that for non-uniform axial stress distributions the experimental buckling stresses are greater than for uniform distributions. This is to be expected since there is then less chance that the position of maximum axial stress would coincide with the position where buckling would begin for a uniform stress in the practical shell.

E. Antona and G. Gabrielli: The failure stress expressions adopted in our paper are based only on experimental results. The theoretical result related to the bending load was reported only because of its practical agreement with the experimental one.

The hypothesis advanced by Mr. Johns, based on the theoretical results he mentioned, must be carefully studied. It is actually possible that the discrepancies between compression and bending failure stress would arise from the probability that the generatrix of major stress in bending coincides with the buckling one in compression.

† SEIDE, P., WEINGARTEN, V., 'On the Buckling of Circular Cylinders under Pure Bending,' Trans ASME (Series A), *J App Mech*, p. 112, March 1961.